Role of diproton correlation in two-proton-emission decay of the ^{6}Be nucleus

Tomohiro Oishi,[1,2,3,4] Kouichi Hagino,[1,2] and Hiroyuki Sagawa[5,6]
[1]*Department of Physics, Tohoku University, Sendai 980-8578, Japan*
[2]*Research Center for Electron Photon Science, Tohoku University, 1-2-1 Mikamine, Sendai 982-0826, Japan*
[3]*Helsinki Institute of Physics, P.O. Box 64, FI-00014 University of Helsinki, Finland*
[4]*Department of Physics, P.O. Box 35 (YFL), University of Jyväskylä, FI-40014 Jyväskylä, Finland*
[5]*Center for Mathematics and Physics, University of Aizu, Aizu-Wakamatsu, Fukushima 965-8560, Japan*
[6]*RIKEN Nishina Center, Wako 351-0198, Japan*
(Received 14 April 2014; published 4 September 2014)

We discuss a role of diproton correlation in two-proton emission from the ground state of a proton-rich nucleus, ^{6}Be. Assuming the three-body structure of $\alpha + p + p$ configuration, we develop a time-dependent approach in which the two-proton emission is described as a time evolution of a three-body metastable state. With this method, the dynamics of the two-proton emission can be intuitively discussed by monitoring the time dependence of the two-particle density distribution. With a model Hamiltonian which well reproduces the experimental two-proton decay width, we show that a strongly correlated diproton emission is a dominant process in the early stage of the two-proton emission. When the diproton correlation is absent, the sequential two-proton emission competes with the diproton emission, and the decay width is underestimated. These results suggest that the two-proton emission decays provide a good opportunity to probe the diproton correlation in proton-rich nuclei beyond the proton dripline.

DOI: 10.1103/PhysRevC.90.034303 PACS number(s): 21.10.Tg, 21.45.−v, 23.50.+z, 27.20.+n

I. INTRODUCTION

The pairing correlation plays an essential role in many phenomena of atomic nuclei [1–5]. In recent years, the dineutron and diproton correlations have particularly attracted a lot of interest in connection to the physics of unstable nuclei [6–15]. These are correlations induced by the pairing interaction, with which two nucleons are spatially localized. Because the pairing gap in infinite nuclear matter takes a maximum at the density lower than the normal density [5,12,16,17], the dinucleon correlation is enhanced on the surface of nuclei. This property may also be related to the BCS-BEC crossover [12,17,18].

Although the dinucleon correlation has been theoretically predicted for some time, it is still an open issue to probe it experimentally. For this purpose, a pair-transfer reaction [19–21] and the electromagnetic excitations [22–28] may be considered. However, even though there have been a few experimental indications [23], so far no direct experimental evidence for the dinucleon correlation has been found, mainly owing to a difficulty to access the intrinsic structures in bound nuclei without disturbing with an external field.

This difficulty may be overcome by using two-proton ($2p$)-emission decays (these are referred to as two-proton radioactivities when the decay width is sufficiently small) of nuclei outside the proton dripline [29–31]. An attractive feature of the $2p$ emission is that two protons are emitted spontaneously from the ground state of unbound nuclei, and thus they are expected to carry information on the pairing correlations inside nuclei, including the diproton correlation [32–35].

The $2p$ radioactivity was predicted for the first time by Goldansky [36,37]. He introduced the concept of the "true $2p$ decay," which takes place in the situation where the emission of a single proton is energetically forbidden. The pairing interaction plays an important role to generate such a situation, lowering the energy of even-Z nuclei. In the true $2p$-decay process, the two protons may be emitted simultaneously as a diproton, that is, the diproton decay [36–38]. This process should thus intimately be related to the diproton correlation.

Since the time of Goldansky, there has been enormous progress in the problem of $2p$ decays, both experimentally and theoretically, and our understanding of the $2p$ decays has been considerably improved [29–31]. It has been considered now that the actual $2p$ decays are often much more complicated than the simple diproton decays that Goldansky originally proposed [39–47]. Moreover, it has not been completely clarified whether the diproton correlation can be actually probed by observing $2p$ decays.

The aim of this paper is to investigate the role of the diproton correlation in $2p$ emissions and discuss a possibility of probing the diproton correlation through the $2p$ decays. For this purpose, one needs to handle a many-body metastable state, for which the theoretical frameworks can be categorized into two approaches: the time-independent framework [48–50] and the time-dependent framework [48,51,52]. In the time-independent approach, the decay state is regarded as a pure outgoing state with a complex energy, that is, the Gamow state. The real and the imaginary parts of the complex energy are related to the decay energy and width, respectively. An advantage of this method is that the decay width can be accurately calculated even when the width is extremely small [31,53–55]. In the time-dependent framework, however, the quantum decay of a metastable state is treated as a time evolution of a wave packet [56–62]. An advantage of this method is that the decay dynamics can be intuitively understood by monitoring the time evolution of the wave packet. These two approaches are thus complementary to each other.

In this paper, we employ the time-dependent approach. This approach has been used in Refs. [56–59] to study

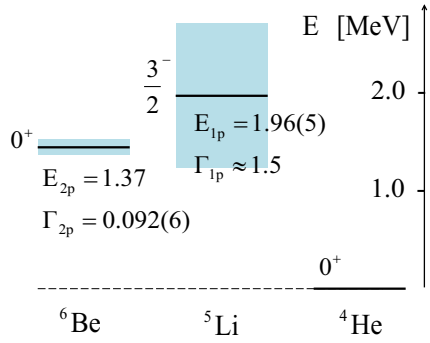

FIG. 1. (Color online) The experimental energy scheme of ^{6}Be and ^{5}Li nuclei with respect to the ground state of ^{4}He [63]. The energies and widths are shown in units of MeV.

one-proton emission decays of proton-rich nuclei. In our previous work [35], we extended this approach to $2p$ emission in one dimension. We here apply this method to a realistic system, that is, the ground state of the ^{6}Be nucleus, by assuming the three-body structure of $\alpha + p + p$. The ^{6}Be nucleus is the lightest $2p$ emitter, where the $2p$-emission decay from its ground state has been experimentally studied in Refs. [39–42]. The experimental Q value of the $2p$ emission is 1.37 MeV [63,64], while the ^{5}Li nucleus is unbound by 1.96(5) MeV from the threshold of $\alpha + p$ [63], as shown in Fig. 1. Although the ^{5}Li nucleus has a large resonance width of about 1.5 MeV [63,64], the ^{6}Be nucleus is considered to be a true $2p$ emitter. Therefore, the sequential decay via the $\alpha + p$ subsystem plays a minor role, and the effect of the diproton correlation, owing to the pairing correlation, may significantly be revealed.

The paper is organized as follows. In Sec. II, we present the theoretical model and the time-dependent approach within a quantum three-body model. The calculated results for ^{6}Be are shown in Sec. III. We also discuss the role of pairing correlation in the $2p$ emission. We then summarize the paper in Sec. IV.

II. FORMALISM

A. Three-body model Hamiltonian

To describe the $2p$ emission from the ground state of ^{6}Be, we consider a three-body model which consists of an α particle as the spherical core nucleus and two valence protons. As in Refs. [8,13,14,27], we employ the so called V coordinate indicated in Fig. 2. Subtracting the center-of-mass motion of the whole nucleus, the total Hamiltonian reads

$$H_{3b} = h_1 + h_2 + \frac{\boldsymbol{p}_1 \cdot \boldsymbol{p}_2}{A_c m} + v_{pp}(\boldsymbol{r}_1, \boldsymbol{r}_2), \tag{1}$$

$$h_i = \frac{\boldsymbol{p}_i^2}{2\mu} + V_{cp}(r_i) \quad (i = 1,2), \tag{2}$$

where h_i is the single-particle (s.p.) Hamiltonian between the core and the ith proton. $\mu \equiv mA_c/(A_c + 1)$ is the reduced mass where m and A_c are the nucleon mass and the mass number of the core nucleus, respectively. The interaction between α and a valence proton, V_{cp}, consists of the nuclear

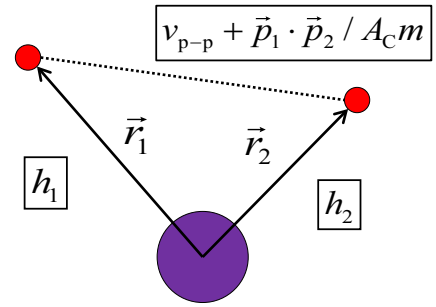

FIG. 2. (Color online) The V coordinate for three-body system.

potential V_{WS} and the Coulomb potential V_{Coul},

$$V_{cp}(r_i) = V_{WS}(r_i) + V_{Coul}(r_i). \tag{3}$$

For the Coulomb part of the potential, V_{Coul}, we use the one appropriate to a uniformly charged spherical α particle of radius $r_c = 1.68$ fm. For the nuclear part, V_{WS}, we use the Woods-Saxon parametrization given by

$$V_{WS}(r) = V_0 f(r) + U_{ls}(\boldsymbol{l} \cdot \boldsymbol{s}) \frac{1}{r} \frac{df(r)}{dr}, \tag{4}$$

where

$$f(r) = \frac{1}{1 + e^{(r-R_0)/a_0}}, \tag{5}$$

with $R_0 = r_c$ and $a_0 = 0.615$ fm. We use the depth parameters of $V_0 = -58.7$ MeV and $U_{ls} = 46.3$ MeV fm^2. This potential yields the resonance energy and the width of the $(p_{3/2})$ channel for α-p scattering of $E_r(p_{3/2}) = 1.96$ MeV and $\Gamma_r(p_{3/2}) = 1.56$ MeV, respectively. These values are compared with the experimental data, $E_r(p_{3/2}) = 1.96(5)$ MeV and $\Gamma_r(p_{3/2}) \sim 1.5$ MeV (see Fig. 1) [63]. We note that this resonance state is quite broad and there has been some ambiguity in the observed decay width [63–66].

For the proton-proton interaction, v_{pp}, we use the Minnesota potential [67] together with the Coulomb term for point charges,

$$v_{pp}(\boldsymbol{r}_1, \boldsymbol{r}_2) = v_0 e^{-b_0 r_{12}^2} + v_1 e^{-b_1 r_{12}^2} + \frac{e^2}{r_{12}}, \tag{6}$$

where $r_{12} = |\boldsymbol{r}_1 - \boldsymbol{r}_2|$. For b_0, b_1, and v_1, we use the same parameters introduced in the original paper [67], as summarized in Table I. However, the strength of the repulsive term, v_0, is adjusted so as to reproduce the empirical Q value for the two-proton emission, as we discuss in Sec. III.

TABLE I. The values of b_0, b_1, and v_1 in the Minnesota potential given by Eq. (6). S indicates the coupled spin of the two protons.

	b_0 (fm^{-2})	b_1 (fm^{-2})	v_1 (MeV)
$S = 0$	1.48	0.639	−178.0
$S = 1$	1.48	0.465	−91.85

B. Uncorrelated two-proton basis

Each s.p. state satisfying $h_i\phi_a(\boldsymbol{r}_i) = \epsilon_a\phi_a(\boldsymbol{r}_i)$ is labeled by $a = \{n_a, l_a, j_a, m_a\}$, that is, a combination of the radial quantum number n, the orbital angular momentum l, the spin-coupled angular momentum j, and its z component m. Using these s.p. wave functions, one can construct the uncorrelated basis for the two protons coupled to an arbitrary spin-parity, J^π, where the coupled angular momentum J is given by $J = j_a \oplus j_b$ and the total parity π is given by $\pi = (-)^{l_a+l_b}$. That is,

$$\Phi_{ab}^{(J^\pi)}(\boldsymbol{r}_1,\boldsymbol{r}_2) = \hat{\mathcal{A}}[\phi_a(\boldsymbol{r}_1)\otimes\phi_b(\boldsymbol{r}_2)]^{(J^\pi)}, \tag{7}$$

where $\hat{\mathcal{A}}$ is the antisymmetrization operator. In this work, we assume that the core nucleus always stays in the ground state with the spin parity of 0^+. Thus, the uncorrelated basis given by Eq. (7) are reduced only to the $J^\pi = 0^+$ subspace, because the ground state of ^{6}Be also has the spin parity of 0^+. That is,

$$\Phi_{ab}^{(0^+)}(\boldsymbol{r}_1,\boldsymbol{r}_2) = \Phi_{n_an_blj}(\boldsymbol{r}_1,\boldsymbol{r}_2) \tag{8}$$

$$= \frac{1}{\sqrt{2\left(1+\delta_{n_a,n_b}\right)}}\sum_m C(j,m;j,-m\mid 0,0) \times\left[\phi_{n_aljm}(\boldsymbol{r}_1)\phi_{n_blj-m}(\boldsymbol{r}_2) + \phi_{n_aljm}(\boldsymbol{r}_2)\phi_{n_blj-m}(\boldsymbol{r}_1)\right]. \tag{9}$$

Notice $l_a = l_b$, $j_a = j_b$ for the 0^+ state. In the following, for simplicity, we omit the superscript (0^+) and use a simplified notation, $|\Phi_M\rangle$, for the uncorrelated basis given by Eq. (9), where $M = (n_a, n_b, l, j)$.

The eigenstates of the three-body Hamiltonian, H_{3b}, can be obtained by expanding the wave function on the uncorrelated basis,

$$|E_N\rangle = \sum_M U_{NM}\,|\Phi_M\rangle\,, \tag{10}$$

where the expansion coefficients, U_{NM}, are determined by diagonalizing the Hamiltonian matrix for H_{3b}. The state $|E_N\rangle$ then satisfies $H_{3b}\,|E_N\rangle = E_N\,|E_N\rangle$ in a truncated space.

All our calculations are performed in the truncated space defined by the energy cutoff, $\epsilon_a + \epsilon_b \leqslant E_{\rm cut} = 40$ MeV. The continuum s.p. states are discretized within the radial box of $R_{\rm box} = 80$ fm (notice that the states $|E_N\rangle$ are also discretized). For the angular momentum channels, we include from $(s_{1/2})^2$ to $(h_{11/2})^2$ configurations. To take into account the effect of the Pauli principle, we exclude the bound $1s_{1/2}$ state from Eq. (10), which is given by the protons in the core nucleus. We have confirmed that our conclusions do not change even if we employ a larger value of $E_{\rm cut}$ and/or include higher partial waves.

C. Time-dependent method for two-proton decay

Assuming the $2p$ emission as a time-dependent process, we carry out time-dependent calculations for the three-body system, ^{6}Be. For this purpose, we first need to determine the initial state, $|\Psi(t=0)\rangle$, for which the two valence protons are confined inside the potential barrier generated by the core nucleus. That is, the $2p$-density distribution at $t = 0$ has almost no amplitude outside the potential barrier. To construct such initial state, we employ the confining potential method, which is detailed in the next section.

The initial state so obtained can be expanded with the eigenstates of H_{3b}, that is, $|E_N\rangle$ given by Eq. (10) as

$$|\Psi(0)\rangle = \sum_N F_N(0)\,|E_N\rangle\,. \tag{11}$$

After the time evolution with the three-body Hamiltonian H_{3b}, this state is evolved to

$$|\Psi(t)\rangle = \exp\left[-it\frac{H_{3b}}{\hbar}\right]|\Psi(0)\rangle = \sum_N F_N(t)\,|E_N\rangle\,, \tag{12}$$

where

$$F_N(t) = e^{-itE_N/\hbar}F_N(0). \tag{13}$$

Notice that the state $|\Psi(t)\rangle$ can also be expanded on the uncorrelated basis as

$$|\Psi(t)\rangle = \sum_M C_M(t)\,|\Phi_M\rangle\,, \tag{14}$$

with

$$C_M(t) = \sum_N F_N(t)U_{NM}. \tag{15}$$

We define the Q value of the $2p$ emission as the expectation value of the total Hamiltonian, H_{3b}, with respect to the initial state, $|\Psi(0)\rangle$. Because the time-evolution operator, $\exp[-itH_{3b}/\hbar]$, in Eq. (12) commutes with H_{3b}, the Q value is conserved during the time evolution. That is,

$$Q = \langle\Psi(0)\,|\,H_{3b}\,|\,\Psi(0)\rangle = \langle\Psi(t)\,|\,H_{3b}\,|\,\Psi(t)\rangle\,. \tag{16}$$

We also note that the wave function is normalized at any time: $\langle\Psi(t)\,|\,\Psi(t)\rangle = 1$.

To extract the information on the dynamics of two-proton emission, it is useful to introduce the decay state, $|\Psi_d(t)\rangle$, which is defined as the orthogonal component of $|\Psi(t)\rangle$ to the initial state [34]. That is,

$$|\Psi_d(t)\rangle \equiv |\Psi(t)\rangle - \beta(t)\,|\Psi(0)\rangle\,, \tag{17}$$

where $\beta(t) = \langle\Psi(0)\,|\,\Psi(t)\rangle$. While the initial state is almost confined inside the potential barrier, the main part of the decay state is located outside the barrier. We define the decay probability as the norm of the decay state,

$$N_d(t) \equiv \langle\Psi_d(t)\,|\,\Psi_d(t)\rangle = 1 - |\beta(t)|^2\,. \tag{18}$$

Notice that $N_d(0) = 0$ because $\beta(0) = 1$. Because $|\beta(t)|^2$ is identical to the survival probability for the decaying process, the decay width can be defined with $N_d(t)$ as [56–59],

$$\Gamma(t) \equiv -\hbar\frac{d}{dt}\ln\left[1 - N_d(t)\right] = \frac{\hbar}{1-N_d(t)}\frac{d}{dt}N_d(t). \tag{19}$$

It is worthwhile to mention that if the time evolution follows the exponential decay law, such that

$$[1 - N_d(t)] = e^{-t/\tau}, \tag{20}$$

then $\Gamma(t)$ is related to the lifetime of the metastable state: $\Gamma = \hbar/\tau$. This situation is realized when the energy spectrum, defined by $\{|F_N(t)|^2\}$, is well approximated as a Breit-Wigner distribution [51,52].

It is useful to define also the partial decay width $\Gamma_s(t)$ to understand the decay dynamics. This is defined as the width for the decay to a channel s, where the total decay width is given by

$$\Gamma(t) = \sum_s \Gamma_s(t). \tag{21}$$

The partial decay width can be calculated with the expansion coefficient $a_s(t)$ of the decay state with the channel wave function,

$$|\Psi_d(t)\rangle = \sum_s a_s(t)\,|s\rangle\,, \tag{22}$$

where $\langle s'\,|\,s\rangle = \delta_{s's}$. Because $N_d(t)$ in Eq. (18) is given as $N_d(t) = \sum_s |a_s(t)|^2$, the partial decay width reads

$$\Gamma_s(t) = \frac{\hbar}{1 - N_d(t)}\frac{d}{dt}N_{d,s}(t), \tag{23}$$

where $N_{d,s} = |a_s(t)|^2$. In the next section, we apply Eq. (23) to calculate the spin-singlet and spin-triplet widths for the $2p$ emission of ^{6}Be.

III. RESULTS

A. Initial state

Let us now numerically solve the three-body model and discuss the $2p$ decay of ^{6}Be. As we mentioned in the previous section, we construct the initial state for the two protons such that the $2p$-density distribution is localized around the core nucleus and thus has almost no amplitude outside the core-proton potential barrier. To this end, we employ the confining potential method [68–70]. Within this method, we modify the core-proton potential, $V_{\rm cp}$, so as to make a metastable two-proton state be bound.

We generate the confining potential for the present problem as follows. Because the α-p subsystem has a resonance at $E_0 = 1.96$ MeV in the $p_{3/2}$ channel, the two protons in ^{6}Be are expected to have a large component of the $(p_{3/2})^2$ configuration. Thus, we first modify the core-proton potential for the $p_{3/2}$ channel to generate a bound state as follows:

$$\begin{aligned} V_{\rm cp}^{\rm conf}(r) &= V_{\rm cp}(r) \quad (r \leqslant R_b), \\ &= V_{\rm cp}(R_b) \quad (r > R_b). \end{aligned} \tag{24}$$

The value of R_b can be chosen somewhat arbitrarily as long as $V_{\rm cp}(R_b)$ is larger than the resonance energy in the $p_{3/2}$ channel. When this condition is satisfied, the modified potential holds a bound state, which resembles the resonance state of the original potential. The accuracy of the calculations is improved if R_b is chosen such that $V_{\rm cp}(R_b)$ is as close as possible to the resonance energy. With this consideration, we have taken R_b to be 5.7 fm, which is outside the potential barrier rather than the barrier position [70]. Even if another value of R_b is employed, the calculations would qualitatively remain the same as long as the initial state is well confined inside the modified potential, although the decay width will be slightly altered.

For the s.p. channels other than $p_{3/2}$, we define the confining potential as

$$V_{\rm cp}^{\rm conf}(r) = \begin{cases} V_{\rm cp}(r) & (r \leqslant R_b), \\ V_{\rm cp}(r) + \Delta V_{p_{3/2}}(r) & (r > R_b), \end{cases} \tag{25}$$

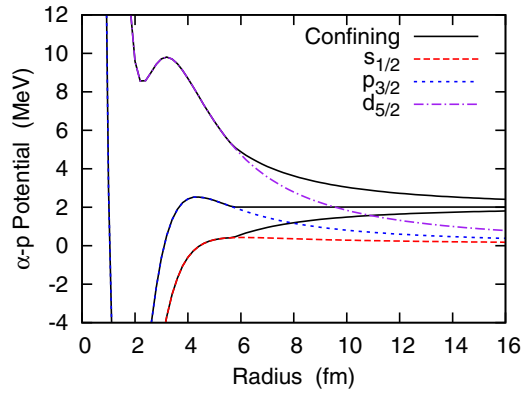

FIG. 3. (Color online) The original and confining potentials for the $s_{1/2}$, $p_{3/2}$, and $d_{5/2}$ channels in the α-p subsystem. R_b in Eqs. (24) and (25) is taken to be 5.7 fm for all the channels.

where $\Delta V_{p_{3/2}}(r) = V_{\rm cp}(R_b) - V_{\rm cp}(r)$ for the $p_{3/2}$ channel. The original and confining potentials for the $s_{1/2}$, $p_{3/2}$, and $d_{5/2}$ channels are shown in Fig. 3. We note that, for this system, the core-proton barrier is mainly attributed to the centrifugal potential rather than the Coulomb potential. This situation is quite different from heavy $2p$ emitters with a large proton number, such as ^{45}Fe.

The initial state for the $2p$ emission is obtained by diagonalizing the modified Hamiltonian including $V_{\rm cp}^{\rm conf}(r)$. The empirical Q value for the two-proton emission is 1.37 MeV for ^{6}Be [63,64]. However, the Minnesota potential with the original parameters overestimates this value by about 50%. Thus, we have modified the parameter v_0 in Eq. (6) from the original value, $v_0 = 200.0$ MeV [67], to $v_0 = 156.0$ MeV so as to yield $Q = 1.37$ MeV when it is calculated by Eq. (16).

In Fig. 4, we show the density distribution of the initial state obtained in this way. By integrating the spin coordinates, the density distribution becomes a function of the radial distances, r_1 and r_2, as well as the opening angle between the two valence protons, θ_{12}. That is,

$$\begin{aligned} &\bar{\rho}_{2p}(t=0; r_1, r_2, \theta_{12}) \\ &\quad \equiv 8\pi^2 r_1^2 r_2^2 \sin\theta_{12}\rho_{2p}(t=0; r_1, r_2, \theta_{12}), \end{aligned} \tag{26}$$

with

$$\rho_{2p}(t=0; r_1, r_2, \theta_{12}) = |\Psi(t=0; r_1, r_2, \theta_{12})|^2\,. \tag{27}$$

Here $\bar{\rho}_{2p}$ is normalized as

$$\int_0^{R_{\rm box}} dr_1 \int_0^{R_{\rm box}} dr_2 \int_0^{\pi} d\theta_{12}\,\bar{\rho}_{2p} = 1. \tag{28}$$

In the top panel of Fig. 4, $\bar{\rho}_{2p}$ is plotted as a function of the distance between the core and the center of mass of the two protons, $r_{\text{c-}pp} = \sqrt{r_1^2 + r_2^2 + 2r_1 r_2\cos\theta_{12}}/2$, and the relative distance between the two protons, $r_{p\text{-}p} = \sqrt{r_1^2 + r_2^2 - 2r_1 r_2\cos\theta_{12}}$. In the bottom panel of Fig. 4, we also display the angular distributions obtained by integrating $\bar{\rho}_{2p}$ for the radial distances.

It is clearly seen that the initial wave function is confined inside the potential barrier at $r \cong 4$ fm (see Fig. 3). Furthermore, the $2p$ density is concentrated near $r_{p\text{-}p} = 2$ fm,

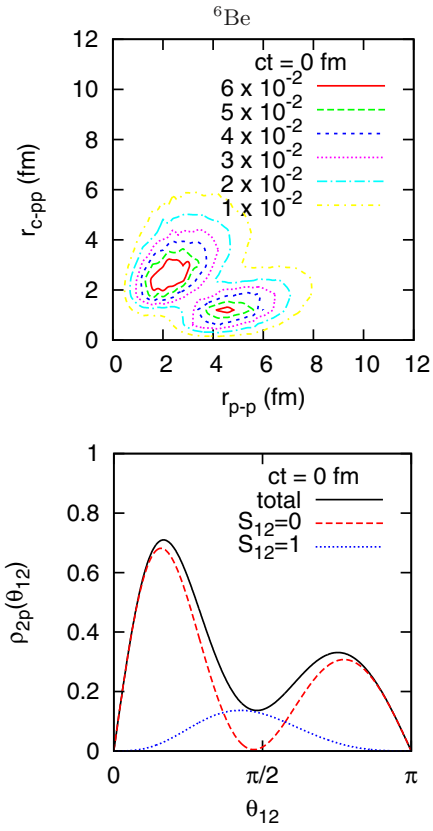

FIG. 4. (Color online) (Top) The $2p$ density at $t = 0$ obtained by including all the configurations up to $(h_{11/2})^2$. It is plotted as a function of $r_{\text{p-p}} = (r_1^2 + r_2^2 - 2r_1r_2\cos\theta_{12})^{1/2}$ and $r_{\text{c-}pp} = (r_1^2 + r_2^2 + 2r_1r_2\cos\theta_{12})^{1/2}/2$. (Bottom) The angular distributions at $t = 0$ obtained by integrating $\bar{\rho}_{2p}$ with respect to r_1 and r_2.

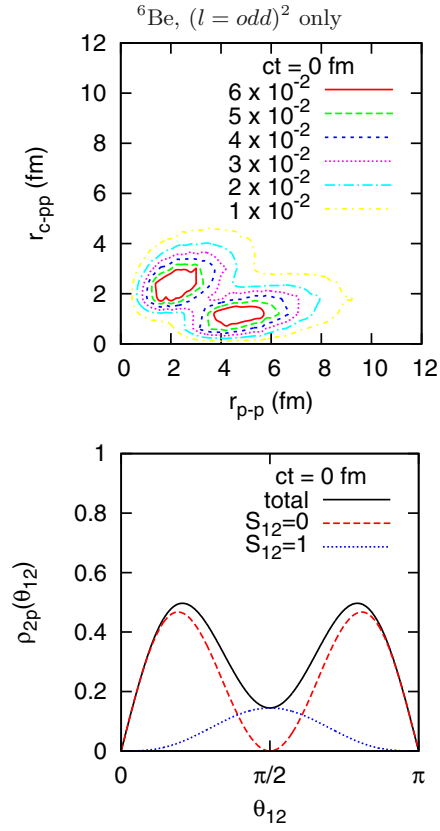

FIG. 5. (Color online) The same as Fig. 4 but in the case with only odd-l partial waves.

corresponding to the diproton correlation in bound nuclei [14]. The corresponding angular distribution becomes asymmetric and has the higher peak at the opening angle $\theta_{12} \cong \pi/6$. This peak is almost attributable to the spin-singlet configuration, being analogous to the dinucleon correlation. This suggests the existence of the diproton correlation in the metastable ground state of ^{6}Be owing to the pairing correlation.

As is well known, the mixture of configurations with odd-l and even-l s.p. states plays an essential role in generating the dinucleon correlation [7]. To study the effect of the diproton correlation in the $2p$ emission, we have also performed the same calculation but only with odd-l partial waves, that is, p^2, f^2, and h^2 in Eq. (9). In the following, we call this case as the $(l = \text{odd})^2$ case. In this case, even though the relative angular momentum between a valence proton and the core nucleus is restricted to be an odd number, the relative angular momentum between the two protons can take both even and odd numbers. Therefore, the pairing correlations are partially taken into account, but only among these s.p. states with odd-l.

In Fig. 5, we show the initial configuration obtained only with the odd-l partial waves. We have used $v_0 = 88.98$ MeV to reproduce the empirical Q value in this case. In the top panel of Fig. 5, there are two comparable peaks at $r_{p\text{-}p} = 2$ and 5 fm, whereas, in the right panel, the corresponding angular distribution has a symmetric form. This result is in contrast with that in the case with all the configurations from $(s_{1/2})^2$ to $(h_{11/2})^2$, shown in Fig. 4, where the pairing correlations are fully taken into account.

In Table II, properties of the initial state are summarized. It is clearly seen that, in the case of the full configuration mixture, the main component is $(p_{3/2})^2$, reflecting the fact that the $p_{3/2}$ channel has a resonance in the α-p subsystem. The mixture of different partial waves are attributed to the off-diagonal matrix elements of H_{3b}, corresponding to the pairing correlations. A comparable enhancement of the spin-singlet configuration

TABLE II. Calculated properties for the initial state of ^{6}Be and the bound ground state of ^{6}He. The results with all the configurations from $(s_{1/2})^2$ to $(h_{11/2})^2$ are labeled by "full." Those obtained only with the odd-l partial waves for ^{6}Be are also shown.

	^{6}Be ($t = 0$)		^{6}He (g.s.)
	Full	$(l = \text{odd})^2$	Full
$\langle H_{3b}\rangle$ (MeV)	1.37	1.37	−0.975
$(p_{3/2})^2$ (%)	88.9	97.1	92.7
$(p_{1/2})^2$ (%)	3.1	2.8	1.6
$(s_{1/2})^2$ (%)	2.2	0.0	1.3
Other $(l = \text{even})^2$ (%)	5.2	0.0	4.2
Other $(l = \text{odd})^2$ (%)	0.6	0.1	0.2
$P(S = 0)$ (%)	82.2	80.6	78.1

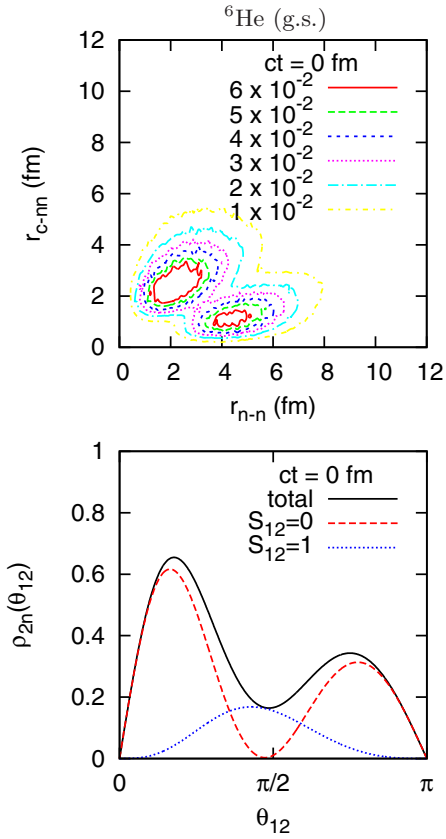

FIG. 6. (Color online) The density distribution of the valence two neutrons, $\tilde{\rho}_{2n}$, in the ground state of ^{6}He. Those are plotted in the same manner as in Fig. 4. The configurations up to $(h_{11/2})^2$ are included.

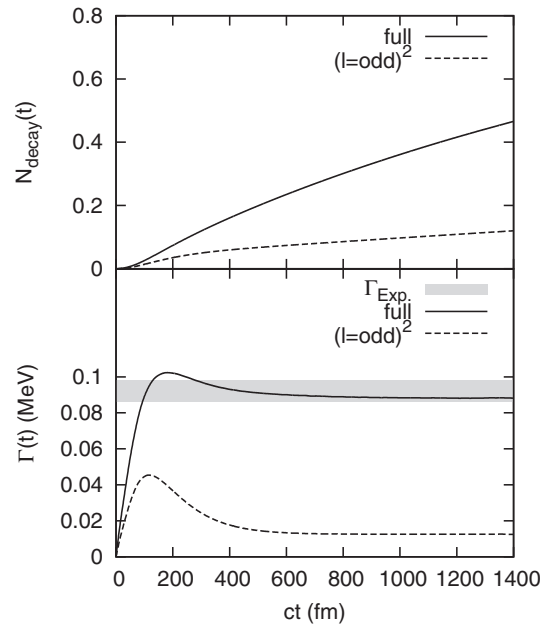

FIG. 7. The decay probability and the decay width of the $2p$ emission from ^{6}Be, obtained with the time-dependent method. The result in the case of the full configuration mixture is plotted by the solid line, whereas that in the $(l = \text{odd})^2$ case is plotted by the dashed line. The experimental value, $\Gamma_{\text{exp}} = 92 \pm 6$ keV [63,64], is marked by the shaded area.

exists also in the case with the $(l = \text{odd})^2$ bases, even though there is no localization of the two protons as shown in Fig. 5.

From the point of view of the isobaric symmetry in nuclei, it is interesting to compare the initial state of ^{6}Be with the ground state of its mirror nucleus, ^{6}He. Assuming the $\alpha + n + n$ structure, we perform the similar calculation for the ground state of ^{6}He. For the α-n system, there is an observed resonance of $p_{3/2}$ at $E_r = 0.735(20)$ MeV with its width, $\Gamma_r = 0.600(20)$ MeV [63,71]. To reproduce this resonance, we exclude the Coulomb term from V_{cp} and modify the depth parameter to $V_0 = -61.25$ MeV in the Woods-Saxon potential. The pairing interaction is adjusted to reproduce the empirical two-neutron separation energy, $\langle H_{3\text{b}} \rangle = -S_{2n} = -0.975$ MeV [71], by using $v_0 = 212.2$ MeV in Eq. (6). Notice that we deal with the bound state of the three-body system in this case, and thus the confining potential is not necessary. In Fig. 6, the two-neutron density distribution is shown in the same manner as in Fig. 4. Its properties are also summarized in the last column of Table II. Obviously, the two-neutron wave function in ^{6}He has a similar distribution to the $2p$-wave function in ^{6}Be. The dinucleon correlation is present also in ^{6}He, characterized as the spatial localization with the enhanced spin-singlet component [13]. Consequently, the confining potential which we employ provides such initial state of ^{6}Be that can be interpreted as the isobaric analog state of ^{6}He.

B. Decay width

To describe the decay process of ^{6}Be, we suddenly change the potential at $t = 0$ from the confining potential, $V_{\text{cp}}^{\text{conf}}$, to the original one, V_{cp}. The initial state constructed in the previous subsection then evolves in time. We first show the results of the decay probability, $N_d(t)$, and the decay width, $\Gamma(t)$, defined by Eqs. (18) and (19), respectively.

In Fig. 7, the calculation is carried out up to $ct = 1400$ fm. We have confirmed that the artifact owing to the reflection at $r = R_{\text{box}}$ is negligible in this time interval. One can clearly see that, after a sufficient time evolution, the decay width converges to a constant value for all the cases, and the exponential decay rule is realized. Furthermore, the result in the case of full configuration mixture yields the saturated value of $\Gamma(t) \cong 88.2$ keV, which reproduces the experimental decay width, $\Gamma = 92 \pm 6$ keV [63,64].

However, the decay width is significantly underestimated when the partial waves are limited only to odd-l partial waves. (Note that we exclude even-l partial waves not only at $t = 0$ but also for $t > 0$ in this case.) The underestimation of the decay width is caused by an increase of the pairing attraction: With the odd-l partial waves only, to reproduce the empirical Q value, we needed a stronger pairing attraction. The two protons are then strongly bound to each other and are difficult to go outside, even if they have a similar energy release to that in the case of full configuration mixture. From this result, we can conclude that the mixing of opposite parity configurations is indispensable to reproduce simultaneously the Q value and the decay width of the $2p$ emission, supporting the assumption of the diproton correlation.

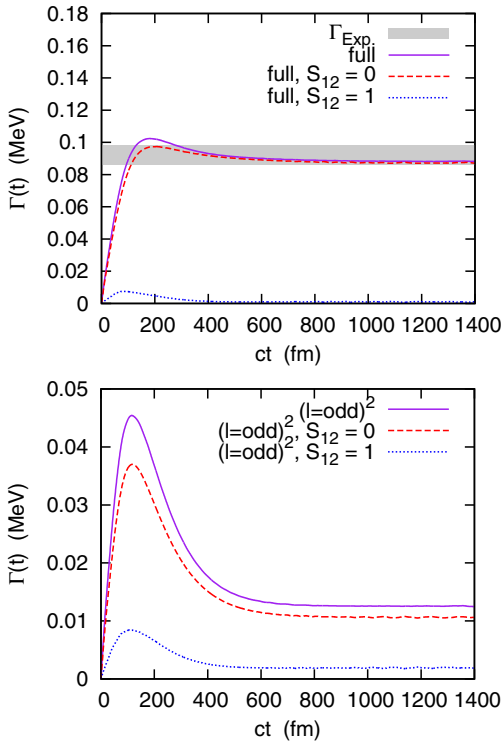

FIG. 8. (Color online) The partial decay widths of the spin-singlet and the spin-triplet configurations in the $2p$ emission of ^{6}Be. In the top panel, the result obtained with all the configurations from $(s_{1/2})^2$ to $(h_{11/2})^2$ is shown. In the bottom panel, the same result but in the case with only odd-l partial waves is plotted.

For the above two cases, we also calculate the partial decay widths for the spin-singlet and the spin-triplet configurations. The corresponding formula to Eq. (23) is given as

$$\Gamma_S(t) \equiv \frac{\hbar}{1 - N_d(t)} \frac{d}{dt} N_{d,S}(t), \tag{29}$$

with

$$N_{d,S}(t) \equiv \langle \Psi_{d,S}(t) \,|\, \Psi_{d,S}(t) \rangle \tag{30}$$

$$= \int_0^{R_{\rm box}} dr_1 \int_0^{R_{\rm box}} dr_2 \int_0^{\pi} d\theta_{12} \times 8\pi^2 r_1^2 r_2^2 \sin\theta_{12} |\Psi_{d,S}(t; r_1, r_2, \theta_{12})|^2, \tag{31}$$

where S indicates the combined spin of the two protons. The results are shown in Fig. 8. Clearly, the spin-singlet configuration almost exhausts the decay width in the case of full configuration mixture shown in the top panel of Fig. 8. This suggests that the emitted two protons from the ground state of ^{6}Be have mostly the $S = 0$ configuration like a diproton. However, in the bottom panel of Fig. 8, one can see that the spin-triplet configuration occupies a considerable amount of the total decay width when we exclude even-l partial waves.

In the first and the second rows of Table III, we tabulate the total and partial widths in the case of full configuration mixture and in the $(l = \text{odd})^2$ cases, respectively. The values are evaluated at $ct = 1200$ fm, where the total widths sufficiently converge. Clearly, there is a significant increase of the spin-singlet width in the case of full configuration-mixture, by about one order of magnitude larger than that in the case of $(l = \text{odd})^2$ waves. However, we get similar values of the spin-triplet width in these two cases. From this result, we can conclude that the mixture of the odd-l and even-l s.p. states is responsible for the enhancement of the spin-singlet emission, although the dominance of the spin-singlet configuration in the initial state is apparent in both cases.

TABLE III. The contributions from the spin-singlet and the spin-triplet configurations to the total decay width. Note that the experimental value of the total decay width is 92 ± 6 keV [63,64]. All the values are evaluated at $ct = 1200$ fm, except those in the "no-pairing" case, which are evaluated at $ct = 3000$ fm. In all the cases, the total energy release (Q value) of the two protons is set to be consistent to the experimental value, 1.37 MeV.

	$\Gamma_{\rm tot}$ (keV)	$\Gamma_{S=0}$ (keV)	$\Gamma_{S=1}$ (keV)
Full	88.2	87.1	1.1
$(l = \text{odd})^2$ only	12.5	10.7	1.8
No-pairing ($ct = 3000$ fm)	348	232	116

A qualitative reason for the dominance of the spin-singlet configuration is attributed to the $(s_{1/2})^2$ channel. Notice that the $(s_{1/2})^2$ channel is allowed only for $S = 0$. Because there is no centrifugal barrier in this channel, the spin-singlet emission can be dominant. However, for the spin-triplet configuration, only $L = 1$ is permitted. Thus, the $(s_{1/2})^2$ configuration does not contribute to it, and there is a centrifugal barrier for all the channels in the spin-triplet configuration. Consequently, apart from the reduction owing to the stronger pairing attraction, the spin-triplet widths are similar in both cases.

C. Time-evolution of decay state

To discuss the dynamics of the emission process, we show the density distribution of the decay state,

$$\bar{\rho}_d(t) = 8\pi^2 r_1^2 r_2^2 \sin\theta_{12} \rho_d(t), \tag{32}$$

$$\rho_d(t) = |\Psi_d(t; r_1, r_2, \theta_{12})|^2 . \tag{33}$$

The decay state, which is orthogonal to the initial state confined inside the potential barrier, has the most of its amplitude outside the potential barrier. In the following, we adopt three sets of radial coordinates: (i) The first set includes $r_{\text{c-}pp}$ and $r_{p\text{-}p}$, similarly to the top panel of Fig. 4. (ii) In the second set, we integrate $\bar{\rho}_d$ with respect to the opening angle, θ_{12}, and plot it as a function of r_1 and r_2. To see the peak structure clearly, we omit the radial weight $r_1^2 r_2^2$ in $\bar{\rho}_d$ in the second set. (iii) Within the third set, however, we integrate $\bar{\rho}_d(t)$ over the radial distances and plot it as a function of θ_{12}. We use in Figs. 10, 11, and 13 these sets of coordinates to present the amplitude of the decay state in actual calculations.

Before we show the results of the actual calculations, we schematically illustrate the dynamic of the $2p$-emissions in Fig. 9. From the geometry, the emission modes are classified into two categories: "simultaneous two-proton" and "one-proton" emissions. The diproton emission is a special case

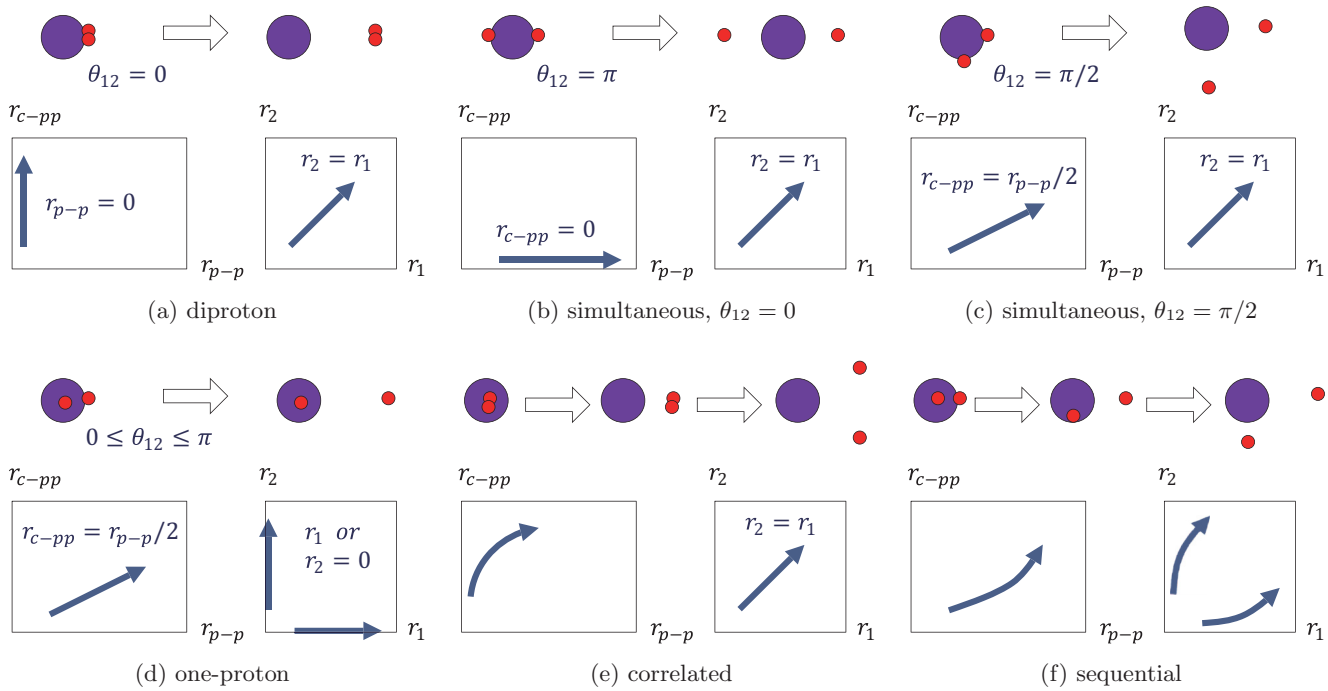

FIG. 9. (Color online) (a)–(c) Schematic illustrations for the trajectories of different $2p$-emission modes. (d) The trajectory of the $1p$ emission. (e),(f) The same as panels (a)–(d) but of the hybrid $2p$ emissions. See the main text for the details.

of the first category. The second category corresponds to the case where only one proton penetrates the barrier.

Figures 9(a)–9(c) correspond to the simultaneous $2p$ emissions with $\theta_{12} = 0,\pi$ and $\pi/2$, respectively, where $\theta_{12} = 0$ [Fig. 9(a)] corresponds to the diproton emission. In these three cases, the density in the (r_1,r_2)-plane shows the same patterns, and is concentrated along $r_1 \cong r_2$. The simultaneous emissions with different opening angles can be distinguished only in the $(r_{p\text{-}p},r_{c\text{-}pp})$ plane: For instance, in the diproton emission, the probability shows mainly along the line with $r_{c\text{-}pp} \gg r_{p\text{-}p}$, while it is along the line with $r_{c\text{-}pp} = 0$ for $\theta_{12} = \pi$. In the one-proton emission shown in Fig. 9(d), only one of the two protons goes through the barrier while the other proton remains inside the core nucleus. This is seen as the increment along $r_{c\text{-}pp} \cong r_{p\text{-}p}/2$ and r_1 or $r_2 \cong 0$ lines.

In Figs. 9(e) and 9(f), we illustrate two hybrid processes. The first one is a "correlated emission," shown in Fig. 9(e). In the correlated emission, the two protons are emitted simultaneously to almost the same direction, holding the diprotonlike configuration. In this mode, in the early stage of tunneling, the density distribution has a larger amplitude in the region with $r_1 \cong r_2$ and small θ_{12}. In the $(r_{p\text{-}p},r_{c\text{-}pp})$ plane, it corresponds to the increment of the probability in the region of $r_{p\text{-}p} \ll r_{c\text{-}pp}$. After the barrier penetration, the two protons separate from each other mainly owing to the Coulomb repulsion. The second hybrid process is a "sequential emission," which is shown in Fig. 9(f). In this mode, there is a large possibility in which one proton is emitted, whereas the other proton remains around the core. The density distribution shows high peaks along $r_1 \gg r_2$ and $r_1 \ll r_2$. In the $(r_{p\text{-}p},r_{c\text{-}pp})$ plane, it corresponds to the increment along the line of $r_{c\text{-}pp} \cong r_{p\text{-}p}/2$. In contrast to the pure one-proton emission, the remaining proton eventually goes through the barrier when the core-proton subsystem is unbound.

1. *Case of full configuration mixture*

We now show the results of the time-dependent calculations for the $2p$ emission of ^{6}Be. We first discuss the case of full configuration mixture, where the odd-l and even-l s.p. states are fully mixed by the pairing correlation. The density distribution for the decay state along the time evolution is shown in Fig. 10. The left, middle, and right columns correspond to the coordinate sets (i)–(iii) defined before, respectively. The first to the fourth panels in each column show the decay density at $ct = 100$, 200, 600, and 1000 fm, respectively. For presentation purposes, we normalize $\bar{\rho}_d$ at each step of time.

In the left and middle columns of Fig. 10, it can be seen that the process in this case is likely the correlated emission shown in Fig. 9(e). Contributions from the other modes shown in Fig. 9 are small. In the middle column of Fig. 10, during the time evolution, there is a significant increment of $\bar{\rho}_d$ along the line with $r_1 \cong r_2$. The corresponding peak in the left column is at $r_{p\text{-}p} \ll r_{c\text{-}pp} \cong 10$ fm, which means a small value of θ_{12}. It should also be noted that, after the barrier penetration, the two protons lose their diprotonlike configuration because of the Coulomb repulsion, which results in the increase of $r_{p\text{-}p}$. Thus, for $r_{c\text{-}pp} \geqslant 10$ fm which is a typical position of the potential barrier from the core, the density distribution extends around the $r_{c\text{-}pp} \cong r_{p\text{-}p}$ region. In this process, the pairing correlation plays an important role to generate the significant diprotonlike configuration before the end of the barrier penetration. In the right column of Fig. 10, the distributions are also displayed as a function of the opening angle, θ_{12}. We can clearly see that the decay state has a high peak at $\theta_{12} \cong \pi/6$ in this time region.

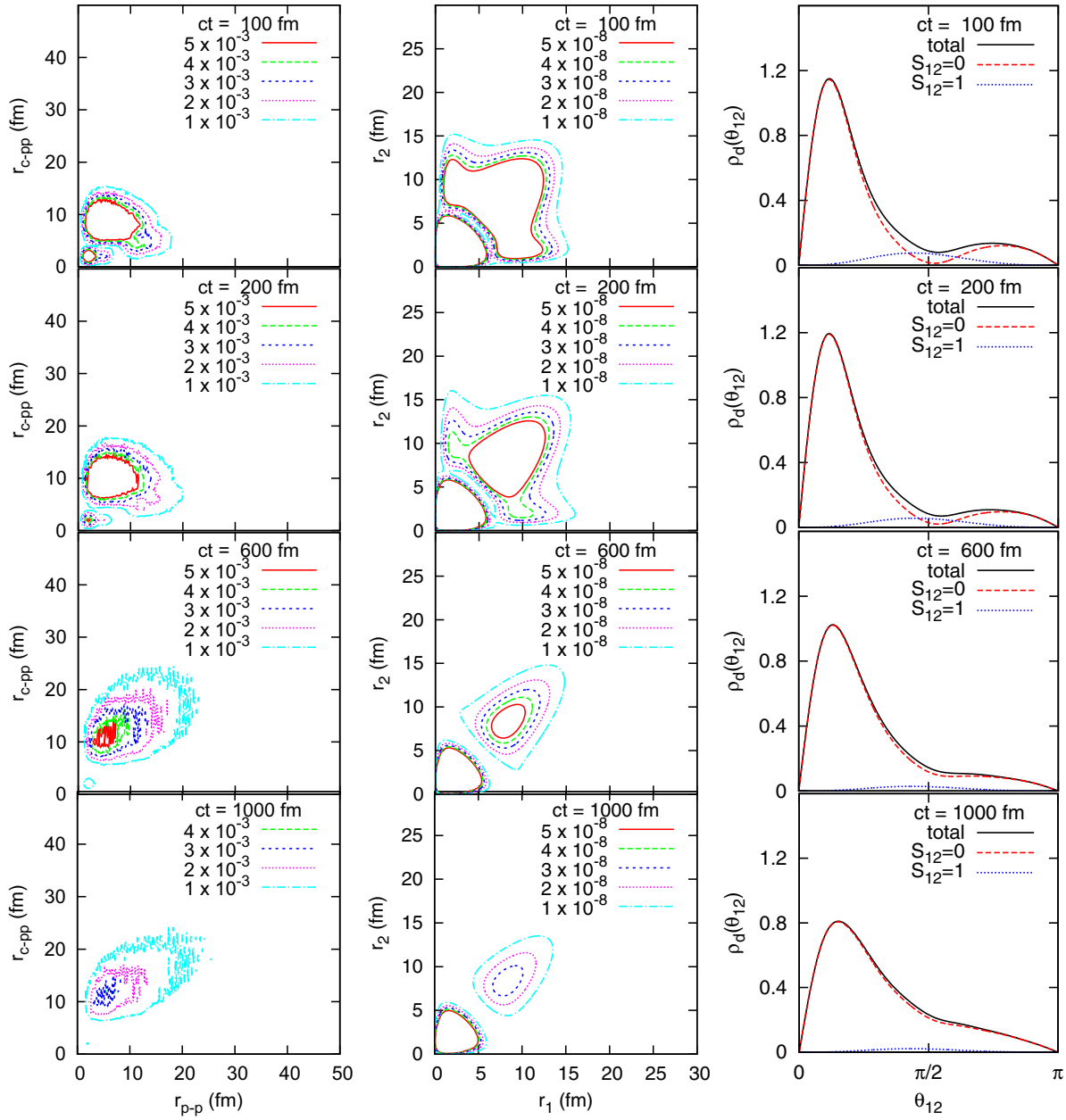

FIG. 10. (Color online) The $2p$-density distribution for the decay states, $\bar{\rho}_d(t)$, obtained with the time-dependent calculations. All the uncorrelated bases up to $(h_{11/2})^2$ are included. (Left column) (i) The distribution as a function of $r_{c\text{-}pp}$ and $r_{p\text{-}p}$. (Middle column) (ii) The distribution as a function of r_1 and r_2, obtained by integrating $\bar{\rho}_d$ for θ_{12}. To clarify the peak(s), the radial weight $r_1^2 r_2^2$ is omitted. (Right column) (iii) The angular distribution of the decay state plotted as a function of the opening angle θ_{12} between the two protons. It is obtained by integrating $\bar{\rho}_d(t)$ for the radial coordinates, r_1 and r_2. Besides the total distribution, the spin-singlet and spin-triplet components are also plotted.

These results imply that the two protons are emitted almost in the same direction, at least in the early stage of the emission process. Intuitively, from the uncertainty principle, this would correspond to a large opening angle in the momentum space. Indeed, such a component has been experimentally observed to be dominant for the $2p$ decay of ^{6}Be [40,41]. It would be an interesting future work to carry out the Fourier transformation of the decay state and compare our calculations with the experimental data.

2. $(l = odd)^2$ case

We next discuss the case only with $(l = \text{odd})^2$ bases. In this case, we only include the uncorrelated basis of p^2, f^2, and h^2 in Eq. (9), both in the initial state and during the time evolution. In Fig. 11, the decay density shows a strong pattern of the sequential emission demonstrated in Fig. 9(f): Significant increments occur along the lines with $r_{c\text{-}pp} \cong r_{p\text{-}p}/2$ and $r_1 \gg r_2$ or $r_1 \ll r_2$. Notice that the contribution from the simultaneous emissions also exists, especially in the early

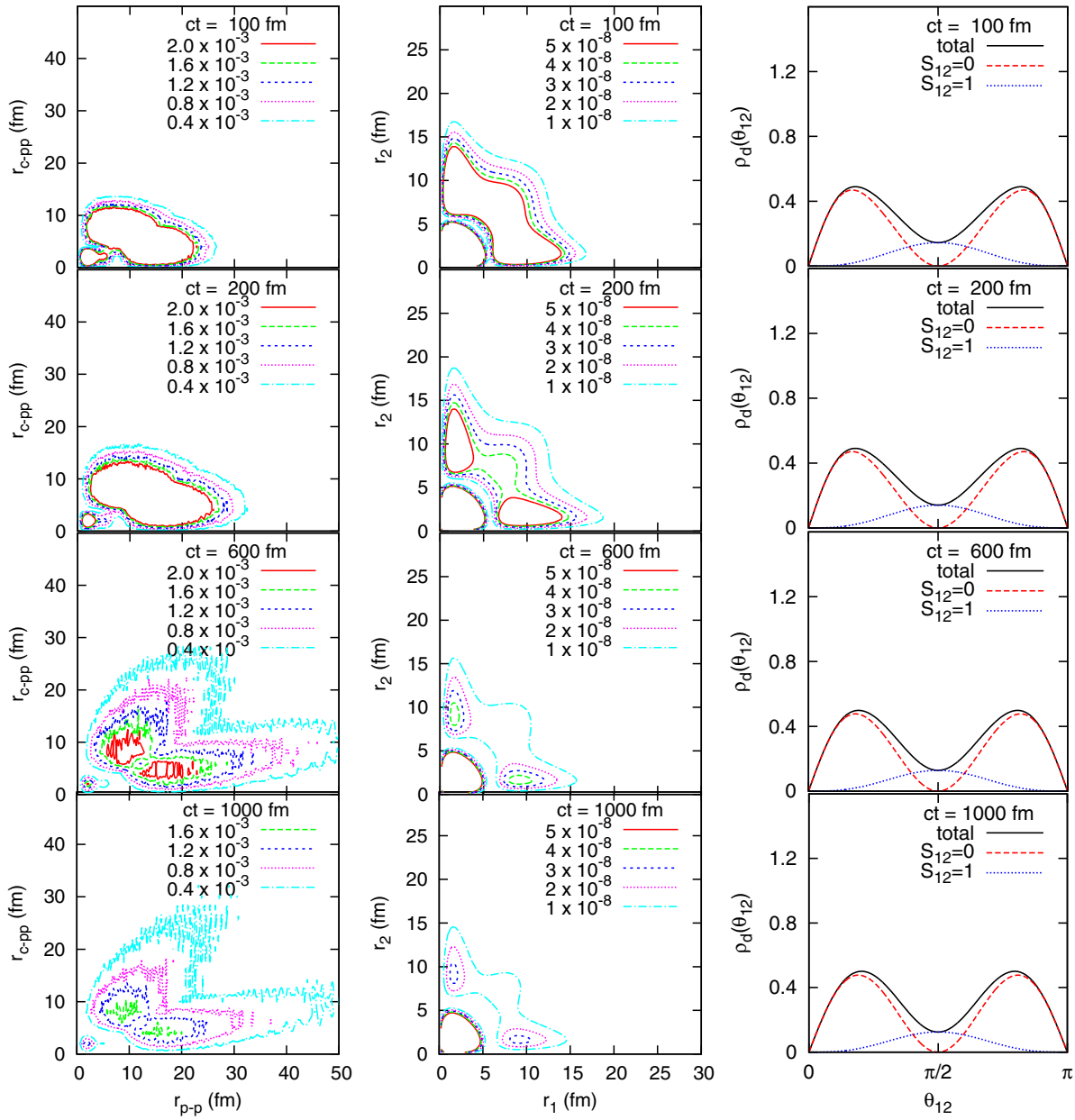

FIG. 11. (Color online) The same as Fig. 10 but for the case with only $(l = \text{odd})^2$ waves. Notice a different scale in the left column from that in Fig. 10.

time region. As a result, the decay state has widely spread amplitudes as a mixture of these emission modes. However, the simultaneous mode is minor compared with the case of full configuration mixture. Notice that the condition for a true $2p$ emitter is satisfied also in this case: The core-proton resonance is located at 1.96 MeV, which is above $Q_{2p} = 1.37$ MeV. However, even with the strong pairing attraction and the energy condition for the true $2p$ emitter, the process hardly becomes the correlated emission when the parity mixing is forbidden or extensively suppressed. The angular distribution shows exactly the symmetric form and is almost invariant during the time evolution. This is because we exclude the pairing correlation between the positive and the negative parity states in the core-proton system, not only at $t = 0$ but also during the time evolution.

3. No-pairing case

Finally, for a comparison with the above two cases, we also perform similar calculations but by completely neglecting the pairing correlation. In this case, we only consider the uncorrelated Hamiltonian, $h_1 + h_2$. Because of the absence of the nondiagonal components in the Hamiltonian matrix, it can be proved that, if the s.p. resonance is at an energy ϵ_0 with its width γ_0, the $2p$ resonance is at $2\epsilon_0$ with its width $2\gamma_0$. The $2p$-wave function is expanded on the uncorrelated basis with a single set of angular quantum numbers. Namely,

$$|\Psi_{(lj)}(t)\rangle = \sum_{n_a,n_b} C_{n_a n_b}(t) \left|\Phi_{n_a n_b lj}\right\rangle, \tag{34}$$

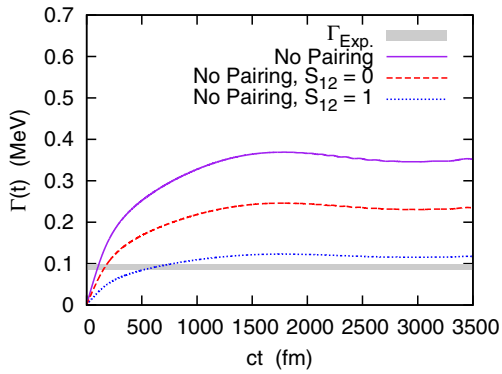

FIG. 12. (Color online) The same as Fig. 8 but for the case without pairing correlations.

where $(lj) = p_{3/2}$ for ^{6}Be. To reproduce the empirical Q value of ^{6}Be, we inevitably modify the core-proton potential. We employ $V_0 = -68.65$ MeV to yield the s.p. resonance at $\epsilon_0(p_{3/2}) = 1.37/2 = 0.685$ MeV, although the scattering data for the core-proton subsystem are not reproduced and the character of a true $2p$ emitter disappears. With this potential, we obtain the s.p. resonance with a broad width: $\gamma_0(p_{3/2}) \cong 170$ keV. Because of the broad decay width, we need to increase the radial box to $R_{\rm box} = 200$ fm to neglect the artifact owing to the reflection at $R_{\rm box}$ in the long time evolution.

The result for the decay width is shown in Fig. 12 and in the last row of Table III. To get the saturated result, we somewhat need a relatively longer time evolution than that in the case of full configuration mixture. Thus, in Table III, we

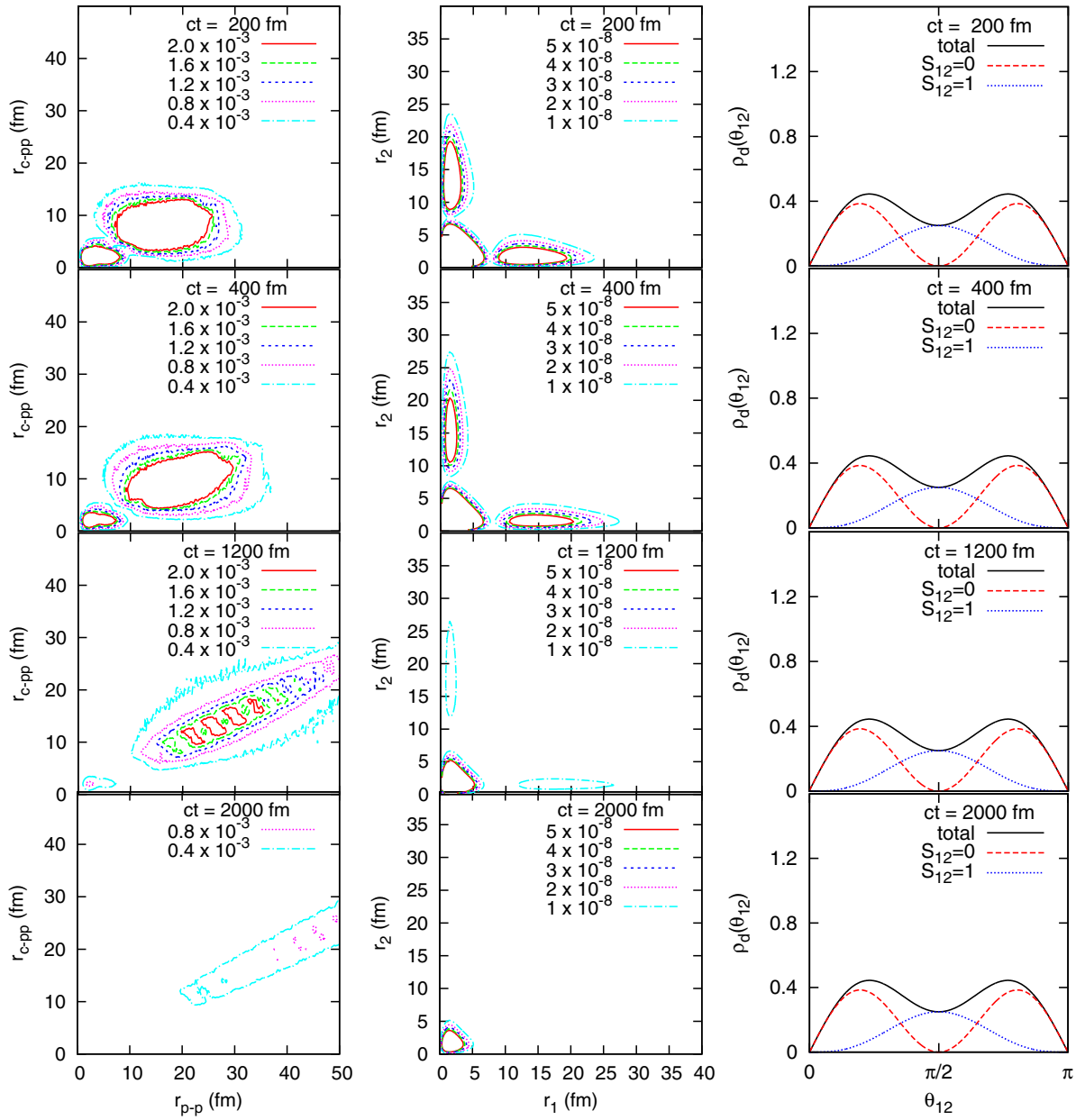

FIG. 13. (Color online) The same as Fig. 10 but for the case without pairing correlations.

evaluate the decay width at $ct = 3000$ fm. By this time, the total decay width, $\Gamma(t)$, converges to about 340 keV, which is consistent to that expected from the s.p. resonance, $\gamma_0(p_{3/2})$. During the time interval shown in Fig. 12, there still remain some oscillations in $\Gamma(t)$. This is a characteristic behavior of the broad resonance, namely an oscillatory deviation from the exponential decay rule. For the spin-singlet and -triplet configurations, their contributions have exactly the ratio of 2 : 1. This result is simply attributed to the recoupling of the angular momentum for the $(p_{3/2})^2$ configuration.

By comparing these results with those in the case of the full configuration-mixing, we can clearly see a decisive role of the pairing correlations in $2p$ emissions. Assuming the empirical Q value, if we explicitly consider the pairing correlations, the decay width becomes narrow and agrees with the experimental data. However, in the no-pairing case, we need a modified core-proton interaction to reproduce the empirical Q value, and the properties of the core-proton resonance state become inconsistent with the experimental data. Even though the Q value is adjusted in this way, the calculated $2p$-decay width is significantly overestimated in this case. Namely, we cannot simultaneously reproduce the experimental Q value and the decay width with the no-pairing assumption. If one is forced to reproduce them simultaneously, one may need an unphysical core-proton interactions.

In Fig. 13, we show the density distribution of the decay state during the time evolution. Obviously, in this case, the process is the sequential or, moreover, like the one-proton emission. There is a significant increase of the density along the lines with $r_{c\text{-}pp} \cong r_{p\text{-}p}/2$ and, consistently, with $r_1 \gg r_2$ and $r_1 \ll r_2$ (see Fig. 9). However, the probability for the simultaneous and correlated emissions are negligibly small. This is quite different from that in the case of full configuration mixture, where the correlated emission is apparent.

D. Role of pairing correlation in decay width

In this section, we discuss a general role of the pairing correlation in the $2p$ emission. To this end, we calculate the $2p$ decay width for different Q values in the case of full configuration mixture and the no-pairing case. The variation of the Q value is done by changing the parameter V_0 in the core-proton potential [Eq. (4)], while the pairing interaction used in the case of full configuration mixture is kept unchanged. Notice that for the no-pairing case, the s.p. resonance appears at $\epsilon_0(p_{3/2}) = Q/2$.

In Fig. 14, the decay width is plotted as a function of the decay Q value. We note that the calculated decay widths are well converged after a sufficient time evolution in all the cases. The decay width is evaluated at $ct = 1200$ and 3000 fm in the full correlation and the no-pairing cases, respectively. Clearly, the no-pairing calculations overestimate the decay width in all the region of Q_{2p}. Namely, the three-body system becomes easier to decay without the pairing correlation, for the same value of the total energy release (Q value). In other words, the pairing correlation plays an essential role in the metastable state, stabilizing it against particle emissions. We note that a similar effect has been predicted also for a one-neutron resonance, that is, the width of a one-neutron

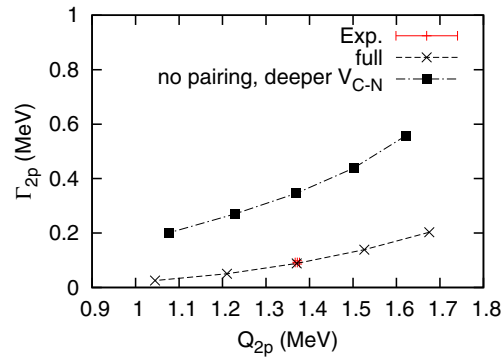

FIG. 14. (Color online) The calculated decay width for the $2p$ emission of ^{6}Be, as a function of the Q value. The Q value is varied by modifying the core-proton potential. The experimental values, $Q_{2p} = 1.372(5)$ MeV and $\Gamma_{2p} = 0.092(6)$ MeV [71], are also indicated.

resonance becomes narrow when one considers the pairing correlations [72].

Also, as we have confirmed in the previous section, the emission dynamics with and without the pairing correlations are essentially different from each other: The correlated emission becomes dominant if the pairing correlation is fully considered, whereas the sequential emission plays a major role in the no-pairing case. Consequently, the pairing correlation must be treated explicitly in the metastable states; otherwise, one would miss the essential effect on both the decay rule and the dynamical phenomena.

IV. SUMMARY

We have investigated the $2p$ emission of the ^{6}Be nucleus by employing a three-body model consisting of an α particle and two valence protons. We have applied the time-dependent method and discussed the decay dynamics of many-body metastale states, particularly in connection to the diproton correlation. An advantage of the time-dependent method is that it provides not only a way to evaluate the decay width, but also an intuitive way to understand the decay dynamics.

By using the confining potential method, we first obtained the initial state of ^{6}Be, in which the two protons are confined inside the potential barrier. Because of the pairing correlation between the two protons, the initial configuration includes the diproton correlation, similarly to the dineutron correlation in the ground states of Borromean nuclei such as ^{6}He. At time $t = 0$, the confinement is removed so that the $2p$ state evolves in space and time. In this calculation, the decay width can be read off by plotting the survival probability as a function of time. We have found that our Hamiltonian well reproduces simultaneously the experimental Q value and decay width of ^{6}Be. We have also shown that the decay state predominantly has the spin-singlet configuration.

By monitoring the time evolution of the density distribution of the decay state, we have confirmed that the decay process in the early stage is mainly the correlated emission, in which the two protons tend to be emitted in a similar direction, reflecting the diproton correlation in the initial state. Thus, the $2p$ emission can be a promising tool to probe experimentally the

diproton correlation. We have also performed the calculations by including only odd-l partial waves to switch off the diproton correlation. In this case, even though we use the model parameters which reproduce the empirical Q value, the decay width is significantly underestimated. The decay process shows a large component of the sequential emission, in contrast to the case of full configuration mixture. From these results, we can conclude that the diproton correlation plays an important role in the $2p$ emission, providing an opportunity to probe it by observing the $2p$ emission.

We have also checked that, if the pairing correlation is completely neglected, the decay width is largely overestimated, partly because the proton-core potential has to be made deeper to yield the empirical Q value. By monitoring the time evolution of the density distribution of the decay state, it has been clarified that the emission is mostly a sequential decay with the no-pairing assumption. Namely, the pairing correlation is critically important to determine not only the decay width but also the dynamical phenomena.

To compare quantitatively the calculated results with the experimental data, we would need a more careful treatment of the final-state interactions (FSIs). In this work, we mainly treat the early stage of the time evolution, terminating the calculations at $ct \sim 1400$ fm to avoid the artifact owing to the reflection at the edge of the box, $R_{\rm box}$. However, the two protons are detected in the actual experiments at a much later time after being significantly affected by the FSIs. To fully take into account the FSIs, we would have to use an extremely large box even though the computational costs would increase severely.

The time-dependent method which we employed in this paper can be applied also to a decay of other many-body metastable states. It provides a novel and intuitive point of view to the decay process. It would be an interesting future problem to apply this method to other problems of many-particle quantum decays, such as the two-neutron emission and the two-electron autoionization of atoms.

ACKNOWLEDGMENTS

We thank M. Matsuo and R. Kobayashi for useful discussions on the effect of the pairing correlation on decay widths. T.O. thanks T. Yamashita in the Cyberscience Center of Tohoku University for a technical help for numerical calculations. This work was supported by the Global COE Program titled "Weaving Science Web beyond Particle-Matter Hierarchy" at Tohoku University, and by a Grant-in-Aid for Scientific Research under Program No. (C) 22540262 by the Japanese Ministry of Education, Culture, Sports, Science and Technology. This work was also supported by Academy of Finland and University of Jyväskylä within the FIDIPRO program.

[1] D. M. Brink and R. A. Broglia, *Nuclear Superfluidity* (Cambridge University Press, Cambridge, U.K., 2005).
[2] P. Ring and P. Schuck, *The Nuclear Many Body Problem* (Springer-Verlag, New York, 1980).
[3] R. A. Broglia and V. Zelevinsky (editors), *Fifty Years of Nuclear BCS: Pairing in Finite Systems* (World Scientific, Singapore, 2013).
[4] J. Dobaczewski, W. Nazarewicz, T. R. Werner, J. F. Berger, C. R. Chinn, and J. Dechargé, Phys. Rev. C **53**, 2809 (1996).
[5] D. J. Dean and M. Hjorth-Jensen, Rev. Mod. Phys. **75**, 607 (2003).
[6] A. B. Migdal, Sov. J. Nucl. Phys. **16**, 238 (1973).
[7] F. Catara, A. Insolia, E. Maglione, and A. Vitturi, Phys. Rev. C **29**, 1091 (1984).
[8] G. F. Bertsch and H. Esbensen, Ann. Phys. (NY) **209**, 327 (1991).
[9] M. V. Zhukov *et al.*, Phys. Rep. **231**, 151 (1993).
[10] Yu. Ts. Oganessian, V. I. Zagrebaev, and J. S. Vaagen, Phys. Rev. Lett. **82**, 4996 (1999); Phys. Rev. C **60**, 044605 (1999).
[11] M. Matsuo, K. Mizuyama, and Y. Serizawa, Phys. Rev. C **71**, 064326 (2005).
[12] M. Matsuo, Phys. Rev. C **73**, 044309 (2006).
[13] K. Hagino and H. Sagawa, Phys. Rev. C **72**, 044321 (2005).
[14] T. Oishi, K. Hagino, and H. Sagawa, Phys. Rev. C **82**, 024315 (2010).
[15] N. Pillet, N. Sandulescu, P. Schuck, and J.-F. Berger, Phys. Rev. C **81**, 034307 (2010).
[16] L. G. Cao, U. Lombardo, and P. Schuck, Phys. Rev. C **74**, 064301 (2006).
[17] J. Margueron, H. Sagawa, and K. Hagino, Phys. Rev. C **76**, 064316 (2007).
[18] K. Hagino, H. Sagawa, J. Carbonell, and P. Schuck, Phys. Rev. Lett. **99**, 022506 (2007).
[19] M. Igarashi, K. Kubo, and K. Yagi, Phys. Rep. **199**, 1 (1991).
[20] W. von Oertzen and A. Vitturi, Rep. Prog. Phys. **64**, 1247 (2001).
[21] H. Shimoyama and M. Matsuo, Phys. Rev. C **84**, 044317 (2011).
[22] N. Fukuda *et al.*, Phys. Rev. C **70**, 054606 (2004).
[23] T. Nakamura *et al.*, Phys. Rev. Lett. **96**, 252502 (2006).
[24] T. Myo, K. Katō, S. Aoyama, and K. Ikeda, Phys. Rev. C **63**, 054313 (2001).
[25] K. Hagino and H. Sagawa, Phys. Rev. C **76**, 047302 (2007).
[26] C. A. Bertulani and M. S. Hussein, Phys. Rev. C **76**, 051602(R) (2007).
[27] T. Oishi, K. Hagino, and H. Sagawa, Phys. Rev. C **84**, 057301 (2011).
[28] Y. Kikuchi, K. Katō, T. Myo, M. Takashina, and K. Ikeda, Phys. Rev. C **81**, 044308 (2010).
[29] B. Blank and M. Ploszajczak, Rep. Prog. Phys. **71**, 046301 (2008).
[30] M. Pfützner *et al.*, Rev. Mod. Phys. **84**, 567 (2012).
[31] L. V. Grigorenko, Phys. Part. Nucl. **40**, 674 (2009).
[32] V. V. Flambaum and V. G. Zelevinsky, J. Phys. G **31**, 355 (2005).
[33] C. A. Bertulani, V. V. Flambaum, and V. G. Zelevinsky, J. Phys. G **34**, 2289 (2007).
[34] C. A. Bertulani, M. S. Hussein, and G. Verde, Phys. Lett. B **666**, 86 (2008).
[35] T. Maruyama, T. Oishi, K. Hagino, and H. Sagawa, Phys. Rev. C **86**, 044301 (2012).

[36] V. I. Goldansky, Nucl. Phys. **19**, 482 (1960).
[37] V. I. Goldansky, Nucl. Phys. **27**, 648 (1961).
[38] D. S. Delion, R. J. Liotta, and R. Wyss, Phys. Rev. C **87**, 034328 (2013).
[39] O. V. Bochkarev *et al.*, Nucl. Phys. A **505**, 215 (1989).
[40] L. V. Grigorenko *et al.*, Phys. Rev. C **80**, 034602 (2009).
[41] L. V. Grigorenko *et al.*, Phys. Lett. B **677**, 30 (2009).
[42] I. A. Egorova *et al.*, Phys. Rev. Lett. **109**, 202502 (2012).
[43] L. V. Grigorenko, I. A. Egorova, R. J. Charity, and M. V. Zhukov, Phys. Rev. C **86**, 061602(R) (2012).
[44] J. Rotureau, J. Okolowicz, and M. Ploszajczak, Phys. Rev. Lett. **95**, 042503 (2005).
[45] K. Miernik *et al.*, Phys. Rev. Lett. **99**, 192501 (2007).
[46] I. Mukha *et al.*, Phys Rev. C **77**, 061303(R) (2008).
[47] I. Mukha *et al.*, Phys Rev. C **82**, 054315 (2010).
[48] A. Bohm, M. Gadella and G. Bruce Mainland, Am. J. Phys. **57**, 1103 (1989).
[49] G. A. Gamov, Z. Phys. **51**, 204 (1928); **52**, 510 (1928).
[50] R. W. Gurney and E. U. Condon, Phys. Rev. **33**, 127 (1929).
[51] N. S. Krylov and V. A. Fock, Zh. Éksp. Teor. Fiz. **17**, 93 (1947).
[52] V. I. Kukulin, V. M. Krasnopolśky, and J. Horácek, *Theory of Resonances* (Kluwer Academic, Dordrecht, 1989).
[53] L. V. Grigorenko, R. C. Johnson, I. G. Mukha, I. J. Thompson, and M. V. Zhukov, Phys. Rev. C **64**, 054002 (2001).
[54] S. Åberg, P. B. Semmes, and W. Nazarewicz, Phys. Rev. C **56**, 1762 (1997).
[55] C. N. Davids and H. Esbensen, Phys. Rev. C **61**, 054302 (2000).
[56] O. Serot, N. Carjan, and D. Strottman, Nucl. Phys. A **569**, 562 (1994).
[57] P. Talou, N. Carjan, and D. Strottman, Phys. Rev. C **58**, 3280 (1998).
[58] P. Talou, D. Strottman, and N. Carjan, Phys. Rev. C **60**, 054318 (1999).
[59] P. Talou, N. Carjan, C. Negrevergne, and D. Strottman, Phys. Rev. C **62**, 014609 (2000).
[60] G. García-Calderón and L. G. Mendoza-Luna, Phys. Rev. A **84**, 032106 (2011).
[61] A. del Campo, Phys. Rev. A **84**, 012113 (2011).
[62] M. Pons, D. Sokolovski, and A. del Campo, Phys. Rev. A **85**, 022107 (2012).
[63] F. Ajzenberg-Selove, Nucl. Phys. A **490**, 1 (1988).
[64] D. R. Tilley *et al.*, Nucl. Phys. A **708**, 3 (2002).
[65] M. Hoefman *et al.*, Phys. Rev. Lett. **85**, 1404 (2000).
[66] A. M. Shirokov, A. I. Mazur, J. P. Vary, and E. A. Mazur, Phys. Rev. C **79**, 014610 (2009).
[67] D. R. Thompson, M. Lemere, and Y. C. Tang, Nucl. Phys. A **286**, 53 (1977).
[68] S. A. Gurvitz and G. Kalbermann, Phys. Rev. Lett. **59**, 262 (1987).
[69] S. A. Gurvitz, Phys. Rev. A **38**, 1747 (1988).
[70] S. A. Gurvitz, P. B. Semmes, W. Nazarewicz, and T. Vertse, Phys. Rev. A **69**, 042705 (2004).
[71] Chart of Nuclides, Database of National Nuclear Data Center (NNDC), http://www.nndc.bnl.gov/chart/.
[72] R. Kobayashi and M. Matsuo (private communication).